Observation of a multiferroic critical end point

Jae Wook Kim[a], S. Y. Haam[a], Y. S. Oh[a], S. Park[b], S.-W. Cheong[b], P. A. Sharma[c], M. Jaime[c], N. Harrison[c], Jung Hoon Han[d], Gun-Sang Jeon[a], P. Coleman[b], and Kee Hoon Kim[a,1]

[a]Center for Strongly Correlated Materials Research and Frontier Physics Research Division, Department of Physics and Astronomy, Seoul National University, Seoul 151-742, South Korea; [b]Rutgers Center for Emergent Materials and Department of Physics and Astronomy, Rutgers University, Piscataway, NJ 08854; [c]National High Magnetic Field Laboratory, Los Alamos National Laboratory, Los Alamos, NM 87545; [d]Department of Physics and BK21 Physics Research Division, Sungkyunkwan University, Suwon 440-746, South Korea

Communicated by Zachary Fisk, University of California, Irvine, July 14, 2009 (received for review August 30, 2008)

The study of abrupt increases in magnetization with magnetic field known as metamagnetic transitions has opened a rich vein of new physics in itinerant electron systems, including the discovery of quantum critical end points with a marked propensity to develop new kinds of order. However, the electric analogue of the metamagnetic critical end point, a "metaelectric" critical end point, has been rarely studied. Multiferroic materials wherein magnetism and ferroelectricity are cross-coupled are ideal candidates for the exploration of this novel possibility using magnetic-field (*H*) as a tuning parameter. Herein, we report the discovery of a magnetic-field-induced metaelectric transition in multiferroic $BiMn_2O_5$, in which the electric polarization (*P*) switches polarity along with a concomitant Mn spin–flop transition at a critical magnetic field H_c. The simultaneous metaelectric and spin–flop transitions become sharper upon cooling but remain a continuous cross-over even down to 0.5 K. Near the *P* = 0 line realized at $\mu_0 H_c \approx 18$ *T* below 20 K, the dielectric constant (ε) increases significantly over wide field and temperature (*T*) ranges. Furthermore, a characteristic power-law behavior is found in the *P*(*H*) and ε(*H*) curves at *T* = 0.66 K. These findings indicate that a magnetic-field-induced metaelectric critical end point is realized in $BiMn_2O_5$ near zero temperature.

spin–flop transition | metaelectric transition | $BiMn_2O_5$

The term "critical end point" refers to a singular point in the phase diagram of matter at the end of a first order phase line, as for example, the liquid–gas critical point of water. The importance of this special point for broad classes of matter has rapidly increased in recent years (1, 2). Not only can it provide large thermal fluctuations as a necessary ingredient for displaying universal power-law of physical quantities, but in the special case where the phase transition is suppressed to zero temperature, it can give rise to intense quantum mechanical fluctuations with a marked propensity to develop instabilities into new kinds of ground state. The latter case has been recently realized in itinerant metamagnets such as $Sr_3Ru_2O_7$ (3) and URu_2Si_2 (4). These developments motivate a parallel search for a metaelectric critical end point. By analogy with magnetism, one might expect sudden cross-overs in electric polarization in the vicinity of a metaelectric critical endpoint to be a rather general phenomenon in (anti)ferroelectric materials under application of an electric field (*E*). However, to date, such metaelectric transitions induced by electric fields have been limitedly observed in specific systems such as relaxor ferroelectrics (5) and $DyVO_4$ with the Jahn–Teller structural distortion (6). One possible reason for the scarcity of the phenomenon is the practical difficulty of applying the large voltages required ($\gtrsim$1 kV) without inducing electrical breakdown. Magnetic fields may in fact be better candidates for inducing metaelectric transitions, because they not only avoid the problem of electrical breakdown but also provide a reversible method of tuning matter with many well-established advantages over alternative methods such as pressure or chemical doping. This is still a challenging task because of the intrinsically small cross-coupling between spin and lattice degrees of freedom. However, in a special class of matter called multiferroics, where the cross-coupling between electricity and magnetism is enhanced (7–13), a rare metaelectric transition, as well as critical end point, can be induced by application of magnetic field, as we show in this study.

Among recently discovered multiferroic materials, the family of RMn_2O_5 (*R* = rare earth, Y) are of particular interest because of their large dielectric response under magnetic fields (8). Although $BiMn_2O_5$ is isostructural to RMn_2O_5 (Fig. 1*A*), its magnetic ground state is distinct from those of other RMn_2O_5 compounds. Only $BiMn_2O_5$ remains in a commensurate antiferromagnetic (AF) phase below $T_N \sim 40$ K with a propagation vector of $\mathbf{Q} = (0.5, 0, 0.5)$ (14, 15), while other RMn_2O_5 compounds develop an instability into an incommensurate (IC) AF structure below $T_{IC} \approx 25$ K (14). According to DC magnetization (*M*) (Fig. 2*A*) and neutron diffraction data (15), $BiMn_2O_5$ has a typical AF spin ordering with an easy axis almost parallel to the *a*-axis without showing any signature of a spiral ordering. At T_N, the development of magnetic order is accompanied by the growth of ferroelectric (FE) polarization *P* and a sharp peak in the dielectric constant ε (Fig. 2 *B* and *C*).

Multiferroicity in materials with incommensurate spiral spin ordering is normally accounted for in terms of the "spin-current model" (16). Recent neutron scattering studies of RMn_2O_5 (*R* = Tb, Ho, Y, and Bi) (15, 17, 18) have suggested an alternative "exchange-striction" scenario for this commensurate magnetic system. The AF phase of RMn_2O_5 involves zigzag chains of spins (dashed orange lines in Fig. 1*A*) with a staggered moment lying almost parallel to the Mn^{3+}–O_{ap} bond (where O_{ap} is the apical oxygen in each pyramid). Neutron measurements show that the staggered moment is tilted away from the *a*-axis by about ±8° at low temperatures (15), an effect which is presumably driven by a large single-ion anisotropy in the pyramid and strong AF exchange interactions along the chain (i.e., large J_4 and $J_5 > 0$ in Fig. 1*A*) (17). The effect of stacking AF zigzag chains along the *b*-axis leads to a five member frustrated Mn spin loop in the *ab*-plane: Mn^{4+}–Mn^{3+}–Mn^{3+}–Mn^{4+}–Mn^{3+}. Although the nearest-neighbor magnetic coupling in the loop is antiferromagnetic, the odd number of bonds leads to frustration of the spins, preventing them from being antiparallel on every bond in the loop. Due to the relatively small exchange interaction between Mn^{3+} – Mn^{4+} ions (J_3), the system forms a unique spin ordering pattern (15): Half of the Mn^{3+} – Mn^{4+} spin pairs across neighboring zigzags are approximately antiparallel, whereas the other half are almost parallel. Under this spin arrangement, exchange-striction between the Mn^{3+} – Mn^{4+} spin pairs shifts ions (mostly Mn^{3+} inside pyramids) in a way that optimizes the spin-exchange energy: Ions with antiparallel spins are pulled towards each other (green dashed circle in Fig. 1*A*), while those with parallel spins move apart (red dashed circle) (19). This exchange-striction mechanism then results in canted

Author contributions: S.-W.C. and K.H.K. designed research; J.W.K., S.Y.H., Y.S.O., S.P., P.A.S., M.J., and N.H. performed research; S.-W.C., J.W.K., N.H., J.H.H., G.-S.J., P.C., and K.H.K. analyzed data; and J.W.K., P.C., and K.H.K. wrote the paper.

The authors declare no conflict of interest.

Freely available online through the PNAS open access option.

[1]To whom correspondence should be addressed. E-mail: khkim@phya.snu.ac.kr.

This article contains supporting information online at www.pnas.org/cgi/content/full/0907589106/DCSupplemental.

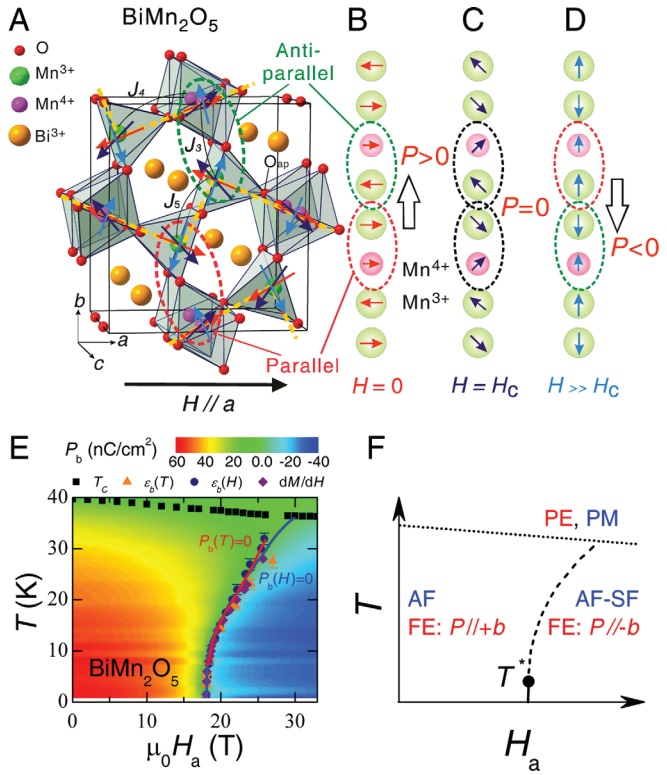

Fig. 1. Magnetic structure and phase diagram. (*A*) The structure and AF zigzag spin chains under various magnetic fields for $BiMn_2O_5$. J_3 and J_4 denote the interchain and intrachain exchange interactions between Mn^{3+}-Mn^{4+} spin pairs, respectively, and J_5 describes that between neighboring Mn^{3+} spins in the bi-pyramid. Red, dark blue, and light blue arrows represent spin directions at $H = 0$, $H = H_c$, and $H \gg H_c$, respectively. (*B-D*) The corresponding simplified spin arrangements and the net P (black open arrows) are shown for $H = 0$ (*B*), $H = H_c$ (*C*), and $H \gg H_c$ (*D*). (*E*) The H–T phase diagram and the intensity contour of P based on the $P(H)$ data. All symbols were determined from the peak positions of $\varepsilon(T)$, $\varepsilon(H)$, and dM/dH. (*F*) Suggested schematic phase diagram. Dotted, solid, and dashed lines indicate the second-order paraelectric (PE)–FE transition, first-order AF to spin-flopped AF (AF–SF) transition, and AF to AF–SF crossover, respectively. A possible critical end point T^* is denoted as a solid circle.

staggered electric dipoles that are aligned parallel to the Mn^{3+}–O_{ap} bond in each bipyramid, leading to an electric polarization P along the b-axis (Fig. 1*B*).

The application of high magnetic fields along the a-axis reveals unexpected magnetic and electric transition features (Fig. 2) at the lowest temperatures, ≈0.5 K; a sharp symmetric peak in the dM/dH curve (Fig. 2*E*) is accompanied by a similar peak in $\varepsilon(H)$ and an abrupt drop in $P(H)$, which passes through zero (Fig. 2 *D* and *F*). This abrupt sign change in P constitutes a metaelectric transition (5, 6). One of the unique features of this electric transition is its tunability with magnetic field H. The critical fields for this metaelectric anomaly, i.e., sign change anomaly of P, increase with temperature and more or less coincide with other anomalies. For example, the temperature of the $\varepsilon(T)$ peaks correspond to the temperature where the polarization $P(T) = 0$ (Fig. 2 *B* and *C*). A contour intensity plot of the $P(H)$ curves (Fig. 1*E*) confirms that the trajectory of the $P(H) = 0$ (blue solid line) closely matches that of the $P(T) = 0$ (red solid line) and the peak positions of $\varepsilon(H)$, dM/dH, and $\varepsilon(T)$ curves below ≈20 K.

We attribute the origin of the sharp magnetic anomaly at $T = 0.5$ K to a spin–flop (SF) transition in the AF zigzag spin chains. This attribution is supported by observations of a small M value and a zero-crossing of the linearly extrapolated line at $H > H_c$, indicating the survival of the AF interaction beyond H_c (Fig. 2*E Inset*). Although the SF is often manifested as a first-order transition, in this case the $M(H)$ curve does not show a clear discontinuity down to 0.5 K, as evidenced by a lack of divergence in the dM/dH curve. This characteristic is also observed in the electric properties; the $P(H)$ curve at 0.66 K shows a sharp decrease but not a clear discontinuity, and the $\varepsilon(H)$ curve does not show divergence even at $T = 0.66$ K except sharpening on cooling. Furthermore, the $\varepsilon(H)$ curves measured in very slow H- or T-sweeps did not show any obvious hysteresis (Supporting information Fig. S1). The lack of a sharp first-order transition feature is more evident in the $P(T)$ curves (Fig. 2*C*), in which P gradually changes its magnitude and sign on cooling. In addition, our preliminary T-dependent specific heat measurements across the $P = 0$ line show no peak structure or discontinuity. These observations strongly suggest that the SF transition and concurrent electrical transition occur via a smooth SF cross-over down to temperatures as low as 0.5 K, during which the spin configuration changes rather continuously from the AF- (Fig. 1*B*) to the SF-type (Fig. 1*D*).

Continuous SF transitions are well-known in antiferromagnets when the magnetic field is applied at an angle to the easy axis: Typically, a SF cross-over occurs when the angle between the field and the staggered moment exceeds a certain critical value (20, 21). This case has been well-studied in uniaxial antiferromagnets such as $GdAlO_3$ (20) and MnF_2 (21). In the former, the critical angle starts from zero at $T_N = 3.2$ K and grows as the temperature is lowered, reaching 10° at zero temperature. So long as the magnetic field inclination exceeds the critical angle, a cross-over is observed, but when the critical angle reaches the field-inclination angle, the system passes through a critical end point, located at a temperature T^* in the H–T plane, and at lower temperatures the SF sharpens into a first-order transition. In SF transitions, the location of T^* is determined as a function of the initial angle between the spin easy axis and the applied field.

We can easily generalize these insights to the case of $BiMn_2O_5$. Fig. 1*A* shows that, in $BiMn_2O_5$, the zigzag chain of Mn spins

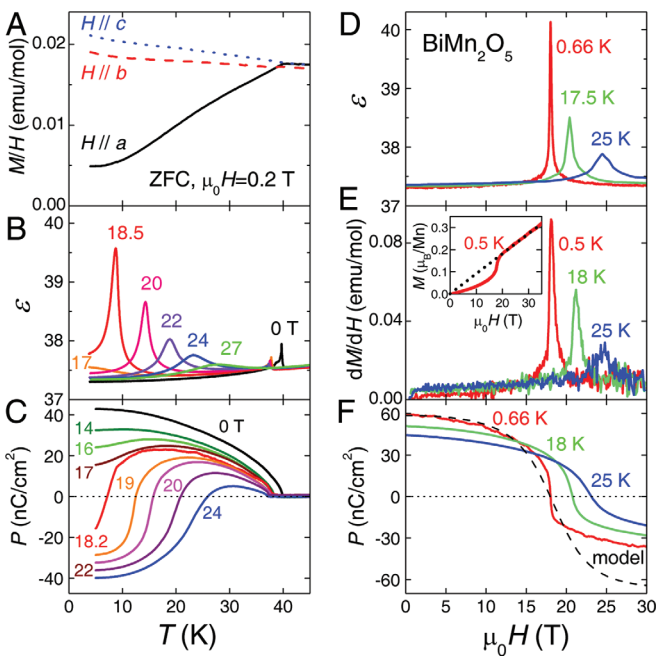

Fig. 2. Electric and magnetic properties of $BiMn_2O_5$. (*A*) M/H measured along the three crystallographic directions. (*B*) $\varepsilon(T)$ data along the b-axis down to 4 K at various magnetic fields applied along the a-axis. The $\varepsilon(H = 0)$ peak near 40 K represents the FE transition. (*C*) $P(T)$ curves at various magnetic fields, showing a cross-over from positive to negative. (*D*) $\varepsilon(H)$ at fixed temperatures. (*E*) dM/dH curves at fixed temperatures. (*Inset*) The $M(H)$ curve at $T = 0.5$ K. (*F*) $P(H)$ at fixed temperatures. The dashed line shows the calculated P curve as predicted by the spin–rotation model described in the text and in Fig. 1. All dotted lines are guides for the eye.

(red arrows) subtend an angle of ±8° to the *a*-axis, providing an intrinsic "tilt" with respect to a field applied along the *a*-axis. In this way, the zigzag chain provides a natural mechanism for a SF cross-over down to some critical temperature T^*. This reasoning leads us to identify the $P = 0$ trajectory in the phase diagram of $BiMn_2O_5$ (Fig. 1*E*) with the SF cross-over line above $T > T^*$. Our data enable us to estimate that the critical temperature T^* is at or below 0.5 K.

One of key findings of this work is the SF cross-over can drive a continuous *H*-induced *P* reversal at $T > T^*$ via the exchange–striction mechanism. To understand the mechanism, consider the effect of a magnetic field on a single AF zigzag chain. If we assume that the interchain coupling (J_3) can be neglected, then the dominant intrachain coupling (J_4 and J_5) will give rise to an almost antiparallel spin alignment. The magnetic free energy of the AF zigzag chain at zero temperature will then be governed by that of a pair of Mn^{3+} spins in the bipyramid, consisting of the energies of the AF spin sublattice and the single-ion anisotropy of the Mn^{3+} spins (22): $F_M = -\mu_0\{\chi_\parallel + (\chi_\perp - \chi_\parallel)\sin^2\theta\}H^2 - \Delta\cos^2(\theta - \theta_0)$. Here, $\chi_\parallel$ and $\chi_\perp$ are magnetic susceptibility values parallel and perpendicular to the staggered moment, respectively. The parameters θ, θ_0, and Δ denote the angle between the Mn^{3+} spin direction and the *a*-axis, the value of θ at zero field, and the single-ion anisotropy energy, respectively. The θ value at each *H* leading to the minimum energy can be obtained from $\partial F_M/\partial\theta = 0$ and the resultant relationship:

$$\tan 2\theta = \frac{\tan 2\theta_0}{1 - \frac{\mu_0(\chi_\perp - \chi_\parallel)}{\Delta\cos 2\theta_0}H^2}. \quad [1]$$

The above equation predicts that when $\theta_0 > 0$ (<0), θ increases (decreases) continuously with *H* to cross the angle 45° (−45°) at $H_c = \sqrt{\Delta\cos 2\theta_0/\mu_0(\chi_\perp - \chi_\parallel)}$. In other words, the spin rotation occurs in a way that each AF zigzag chain rotates counterclockwise or clockwise alternatively to cross 45° or −45° at H_c (dark blue arrows in Fig. 1*A*). When we consider the special ±45° configuration (Fig. 1*C*), in which the angle between Mn^{3+} and Mn^{4+} spins becomes 90°, the exchange–striction is balanced and gives $P = 0$. Upon further increasing *H*, $|\theta|$ increases to make the spin alignment almost perpendicular to the field (blue arrows in Fig. 1*A*). As a result, the relative orientation of neighboring Mn spins reverses as a function of field (see Fig. 1 *B* and *D*) giving rise to the sign reversal in the electric polarization *P*.

For comparison with the experimental data, we have calculated the value of $P \propto \mathbf{S}^{4+} \cdot \mathbf{S}^{3+} \sim\cos 2\theta$ with θ determined in Eq. **1**. Here, $\mathbf{S}^{4+}$ and $\mathbf{S}^{3+}$ are the spin vectors of neighboring Mn ions between the AF zigzag chains. The dashed line in Fig. 2*F* shows the calculated *P*(*H*) curve with $\mu_0 H_c = 18.04$ T and $\theta_0 = 8°$, showing a qualitative agreement with the curve at $T = 0.66$ K. Therefore, the rather continuous magnetic field-induced *P* reversal observed in $BiMn_2O_5$ can be accounted for by the variation of exchange–striction degree driven by the Mn spin–flop cross-over. We further note that only $BiMn_2O_5$ has a homogeneous positive *P* below T_C under small electric poling; all the other RMn_2O_5 develop additional FE domains with negative polarity and antiphase domain wall boundaries below T_{IC} (23). In turn, the above *P* reversal model can be applied to $BiMn_2O_5$ only, and it appears to explain why the experimental finding of *P* reversal as well as the ε increase near H_c are unique to $BiMn_2O_5$ (24).

The magnetically induced polarization reversal we observe is closely analogous to the field-induced metamagnetic transitions observed in spin systems (1, 25) and is most naturally regarded as a magnetic-field induced "metaelectric" transition (6). Because the inversion symmetry is already broken in both sides of the $H_c(T)$ boundary in Fig. 1*F*, the metaelectric transition involves only a change in the magnitude of the ferroelectric order parameter *P*. In this case, due to the coupling of *P* to the Mn spin moment, the metaelectric transition occurs as a cross-over down to very low

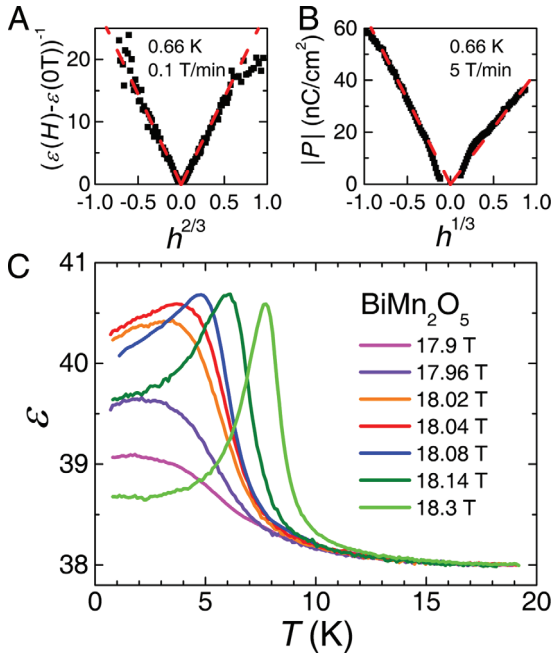

Fig. 3. Field-induced power-law evolution and ε anomaly at very low temperature. (*A*) $(\varepsilon(H) - \varepsilon(H = 0))^{-1}$ vs. $h^{2/3}$, where $h \equiv (H - H_c)/H_c$ and $\mu_0 H_c = 18.04$ T. A very slow ramping rate (0.1 T/min) was used for the ε(*H*) measurement. The red dashed lines are linear guides passing through the origin. The linear relationship was valid in a wide $|h| = 0.004$–0.45 (i.e., $\mu_0|H - H_c| = 0.1$–8 T). (*B*) Plot of $|P|$ vs. $h^{1/3}$. The linear regime of *h* was $|h| = 0.02$–0.45 ($\mu_0|H - H_c| = 0.3$–8 T). To increase the signal-to-noise ratio, it was necessary to choose a rather fast ramping rate (5 T/min) for the *P*(*H*) measurement, which made the *P* data less reliable in a small *h* region. (*C*) Detailed ε(*T*) curves down to *T* ~0.6 K at fixed *H* near H_c. The shape of the ε(*T*) curves above the maximum temperature was similar to that predicted by Barrett's theory (Fig. S2).

temperatures ($T = 0.5$ K). The systematically increased sharpening observed in ε(*H*), dM/dH, and *P*(*H*) curves upon cooling indicate that T^* is close to 0.5 K. If so, we would expect to observe critical fluctuations associated with the critical end point, with a power-law evolution of the physical quantities in close proximity to T^*. Our experiment confirms this expectation as shown in Fig. 3 *A* and *B*, where $(\varepsilon(H) - \varepsilon(H = 0))^{-1}$ vs. $h^{2/3}$ and $|P|$ vs. $h^{1/3}$ plots produce quite linear behavior. Here $h \equiv |(H - H_c)/H_c|$ is the normalized deviation from the critical field $\mu_0 H_c = 18.04$ T. The linearity observed over a broad range of *h* ($|h| = 0.004$–0.45 for ε) means that a single power-law of $P \propto h^{1/3}$ can robustly explain the experimental data, even for *H* very close to H_c. Furthermore, our attempts to fit the data at temperatures above 1.5 K reduce the linearity range for both ε and *P* fits so that the power-law becomes most evident at the lowest temperature available, $T = 0.66$ K, in our experiment.

We find that the peculiar power-law of *P* and ε near T^* can be effectively described by a Landau–Ginzburg-type free energy $F = F_{ME} + F_E$, where

$$F_{ME} = a(\mathbf{S}^{4+} \cdot \mathbf{S}^{3+})P = a(H - H_c)P \quad [2]$$

and

$$F_E = \frac{b}{2}(T - T^*)P^2 + \frac{u}{4}P^4. \quad [3]$$

The magnetoelectric free energy F_{ME} consists of a coupling term between the spin orientations and the electric polarization, whereas the ferroelectric free energy F_E effectively describes the evolution of *P* as a cross-over at $T > T^*$ and as a first-order transition at $T < T^*$ under the assumption that the coefficient of P^2 changes its sign across T^*. The second derivative

of F_E with respect to P determines the dielectric susceptibility $\chi_e^{-1}(P) = b(T - T^*) + 3uP^2$, where $\varepsilon = \chi_e(P) + 1$. The sharp increase in χ_e observed in experiments can be understood as the closeness of the system to the critical end point T^*. In our Landau–Ginzburg model, when the temperature is approximately T^*, the physics is driven by the interplay between the dominant quartic P^4 term and linear P term. Under this assumption, $\partial(F_{ME}+F_E)/\partial P\,|_{E=0} = 0$ provides $P \propto (H-H_c)^{1/3}$. Furthermore, $\partial^2(F_{ME} + F_E)/\partial P^2 \equiv \chi_e^{-1} = 3uP^2 \propto (H - H_c)^{2/3}$. These predicted exponents are consistent with those determined experimentally (Fig. 3 *A* and *B*), clearly supporting the existence of T^* near 0.66 K.

The low value of T^* found in our experiments suggests that $BiMn_2O_5$ lies close to a metaelectric quantum critical point, where T^* is actually zero. Closely analogous behavior is well-known in the case of the itinerant metamagnet $Sr_3Ru_2O_7$ (1). In this respect, several features of the present data particularly prompt further notice. First, the observation of the robust power-law of $P \propto h^{1/3}$ suggests a unique mean-field type while the system is expected to have a 3D Ising universality class ($P \propto h^{1/4.82}$) near the classical critical end point as seen in the liquid–gas transition. Moreover, the trajectory of the cross-over temperature near the zero temperature limit following $(H - H_c)^{1/2}$ (Fig. 1*E*) again constitutes another mean-field type behavior. Thus, all these observations suggest that the effective dimension of the system has been lifted up to 4 or higher so as not to produce the expected 3D fluctuation. One possible origin for such a dimensional increase is in fact the dynamic exponent effect expected due to the prevailing quantum critical end point fluctuation.

The insights gained by our measurements and analysis above suggest that the multiferroic $BiMn_2O_5$ provides a rare opportunity to find a multiferroic quantum critical point and to test its influence on ferroelectric materials. Supporting this conclusion, detailed $\varepsilon(T)$ shape realized near H_c (Fig. 3*C*) further reveals a clue toward detecting the quantum critical signature. When H approaches 18.04 T from below, a systematic increase of $\varepsilon(T =$ 0.66 K) occurs. In particular, at $\mu_0 H_c = 18.04$ T, ε continues to increase as T decreases from 20 K and shows a broad maximum at $\approx$4 K, followed by a slight decrease of 0.5 % down to $\approx$0.6 K. The behavior qualitatively resembles that of the $\varepsilon(T)$ curve in quantum paraelectric systems, such as $SrTiO_3$ (26–29). Furthermore, the increase in $\varepsilon(T)$ between 4 and 20 K is not proportional to the inverse of temperature, as expected in classical paraelectrics. Instead, it is closer to the shape predicted by Barrett's theory (Fig. S2) (30), indicating that the enhanced magnetic fluctuation in close vicinity to the spin–flop T^* can be also linked to the enhanced lattice fluctuation with quantum mechanical population of the relevant phonon mode. This link might be a natural consequence of the existence of dynamic coupling between magnetism and lattice, called as electromagnon (31), in this multiferroic system. Therefore, through this nontrivial coupling channel, the physics of $BiMn_2O_5$ appears to involve quantum zero point lattice motion at low temperatures, as does $SrTiO_3$ see Fig. S3 and *SI Text*. The uniqueness of $BiMn_2O_5$ lies in the magnetic-field-tunability of its quantum-paraelectric properties.

Our observations raise the interesting possibility that instabilities into new quantum states of matter might develop in close vicinity to the multiferroic critical end point, as they do near the magnetic quantum critical end point in $Sr_3Ru_2O_7$. It would be interesting to investigate this possibility by fine-tuning the T^* position, either by by rotating the field direction or by applying external pressure.

Materials and Methods

Single crystal samples were grown using the flux method (8). All the electrical properties were measured along the *b*-axis while the magnetic field was applied along the *a*-axis up to 35 T at the National High Magnetic Field Laboratory. Dielectric constants were measured by a capacitance bridge (GR1615A or AH2500A) at 1 kHz (24). *P* was obtained by integration of the pyro- and magnetoelectric currents measured near an electrometer (Keithley 617). Given the limited magnet time for high-field measurements, the continuous application of a small electric field bias of $E = 2$ kV/cm was quite useful in quickly determining the *P* evolution. In particular, the value of $E = 2$ kV/cm was sufficient to fully polarize the sample on cooling through T_C but small enough to produce a *P* close to its spontaneous value. In several field and temperature sweeps, it was verified that the spontaneous *P* measured under zero electric field after poling with $E = 2$ kV/cm is close to the *P* measured under the same bias. We determined an absolute *P*(*H*) curve under a constant temperature (for Figs. 1*E* and 2*F*) by combining a predetermined *P*(*T*) value at zero or finite *H* and relative changes of *P* under *H* variation from the magnetoelectric current measurements. A precalibrated capacitance sensor was used for accurate *T*-sweeps between 0.6 and 20 K near H_c (Fig. 3*C*), while a Cernox sensor was mostly used for the *T*- and *H*-sweeps above 4 K. For *H*-swept measurements at $T = 0.66$ K and 1.5 K, temperatures were stabilized by controlling the vapor pressure. Specific heat was measured with a plastic calorimeter. Temperature-dependent DC magnetization was measured with a vibrating sample magnetometer in a Physical Property Measurement System (Quantum Design). A pickup-coil magnetometer was used to measure the *H*-dependent magnetization in a pulse magnet at National High Magnetic Field Laboratory of Los Alamos National Laboratory.

ACKNOWLEDGMENTS. We thank P. Chandra, S. Rowley, J. Schmalian, and G. R. Stewart for stimulating discussions. This work was supported by the Korean Government through National Research Laboratory Program M10600000238 and Graduate Partnerships Program K20702020014-07E0200-01410, and by Korea Research Foundation Grant KRF-2008-205-C00101. J.W.K. was supported by Seoul Research and Business Development. Work at Rutgers University was supported by National Science Foundation Grants NSF-0405682 and NSF-DMR-0605935. Work at the National High Magnetic Field Laboratory was performed under the auspices of the National Science Foundation, the State of Florida, and the U.S. Department of Energy.

1. Grigera SA, et al. (2001) Magnetic field-tuned quantum criticality in the metallic ruthenate $Sr_3Ru_2O_7$. *Science* 294:329–332.
2. Harrison N, Jaime M, Mydosh JA (2003) Reentrant hidden order at a metamagnetic quantum critical end point. *Phys Rev Lett* 90:096402.
3. Grigera SA, et al. (2004) Disorder-sensitive phase formation linked to a metamagnetic quantum criticality. *Science* 306:1154–1157.
4. Kim KH, et al. (2004) Nexus between quantum critically and phase formation in $U(Ru_{1-x}Rh_x)_2Si_2$. *Phys Rev Lett* 93:206402.
5. Kutnjak Z, Petzelt J, Blinc R (2006) The giant electromechanical response in ferroelectric relaxors as a critical phenomenon. *Nature* 441:956–959.
6. Vekhter BG, Kaplan MD (1979) A new type of structural Jahn-Teller phase transition in $DyVO_4$ induced by an electric field. *JETP Lett* 29:155–157.
7. Kimura T, et al. (2003) Magnetic control of ferroelectric polarization. *Nature* 426: 55–58.
8. Hur N, et al. (2004) Electric polarization reversal and memory in a multiferroic material induced by magnetic fields. *Nature* 429:392–395.
9. Spaldin NA, Fiebig M (2005) The renaissance of magnetoelectric multiferroics. *Science* 309:391–392.
10. Eerenstein W, Mathur ND, Scott JF (2006) Multiferroic and magnetoelectric materials. *Nature* 442:759–765.
11. Tokura Y (2006) Multiferroics as quantum electromagnets. *Science* 312: 1481–1482.
12. Kenzelmann M, et al. (2007) Direct transition from a disordered to a multiferroic phase on a triangular lattice. *Phys Rev Lett* 98:267205.
13. Picozzi S, et al. (2007) Dual nature of improper ferroelectricity in magnetoelectric multiferroic. *Phys Rev Lett* 99:227201.
14. Muñoz A, et al. (2002) Magnetic structure and properties of $BiMn_2O_5$ oxide: A neutron diffraction study. *Phys Rev B* 65:144423.
15. Vecchini C, et al. (2008) Commensurate magnetic structures of RMn_2O_5 (*R* = Y, Ho, Bi) determined by single-crystal neutron diffraction. *Phys Rev B* 77:134434.
16. Katsura H, Nagaosa N, Balatsky AV (2005) Spin current and magnetoelectric effect in noncollinear magnets. *Phys Rev Lett* 95:057205.
17. Chapon LC, et al. (2004) Structural anomalies and multiferroic behavior in magnetically frustrated $TbMn_2O_5$. *Phys Rev Lett* 93:177402.
18. Chapon LC, et al. (2006) Ferroelectricity induced by acentric spin-density waves in YMn_2O_5. *Phys Rev Lett* 96:097601.
19. Cheong S-W, Mostovoy M (2007) Multiferroics: A magnetic twist for ferroelectricity. *Nat Mater* 6:13–20.
20. Blazey KW, Rohrer H, Webster R (1971) Magnetocaloric effects and the angular variation of the magnetic phase diagram of antiferromagntic $GdAlO_3$. *Phys Rev B* 4:2287–2302.
21. King AR, Rohrer H (1979) Spin-flop bicritical field in MnF_2. *Phys Rev B* 19:5864–5876.
22. Kanamori J (1963) in *Magnetism*, eds Rado GT, Suhl H (Academic, New York), pp 127–203.
23. Koo J, et al. (2007) Non-resonant and resonant X-ray scattering studies on multiferroic $TbMn_2O_5$. *Phys Rev Lett* 99:197601.
24. Haam SY, et al. (2006) Evolution of ferroelectric and antiferromagnetic phases of $TbMn_2O_5$ under high magnetic field up to 45 T. *Ferroelectrics* 336:153–159.
25. Stryjewski E, Giordano N (1977) Metamagnetism. *Adv Phys* 26:487–650.
26. Khmel'nitskii DE, Shneerson VL (1971) Low-temperature displacement-type phase transition in crystals. *Sov Phys Solid State* 13:687–694.
27. Kvyatkovski OE (2001) Quantum effects in incipient and low-temperature ferroelectrics. *Phys Solid State* 43:1401–1419.
28. Wang R, Sakamoto N, Itho M (2000) Effects of pressure on the dielectric properties of $SrTi^{18}O_3$ and $SrTi^{16}O_3$ single crystals. *Phys Rev B* 62:R3577–R3580.
29. Horiuchi S, Okimoto Y, Kumai R, Tokura Y (2003) Quantum phase transition in organic charge-transfer complexes. *Science* 299:229–232.
30. Barrett JH (1952) Dielectric constant in perovskite type crystals. *Phys Rev* 86:118–120.
31. Pimenov A, et al. (2006) Possible evidence for electromagnons in multiferroic manganites. *Nat Phys* 2:97–100.